Surfaces and Interfaces 34 (2022) 102372

Contents lists available at ScienceDirect

Surfaces and Interfaces

journal homepage: www.sciencedirect.com/journal/surfaces-and-interfaces

Investigation of surface-modified EBM printed Ti-6Al-4V alloys for biomedical applications

Selim Demirci [a,b,*], Tuncay Dikici [c,d], Mehmet Masum Tünçay [a], Ramazan Dalmış [e], Nusret Kaya [f], Kürşat Kanbur [g], Fatih Sargın [g], Arif Nihat Güllüoğlu [a]

[a] Faculty of Engineering, Department of Metallurgical and Materials Engineering, Marmara University, Maltepe, Istanbul 34854, Turkey
[b] Institute of Pure and Applied Sciences, Marmara University, Kadikoy, Istanbul 34722, Turkey
[c] Welding Technology Department, Dokuz Eylul University, Torbalı Vocational School, Torbalı, Izmir 35860, Turkey
[d] Center for Fabrication and Application of Electronic Materials, Dokuz Eylul University, Buca, Izmir 35390, Turkey
[e] Faculty of Engineering, Department of Metallurgical and Materials Engineering, Dokuz Eylul University, Buca, Izmir 35390, Turkey
[f] Katip Çelebi University, Faculty of Engineering, Department of Materials Science and Engineering, Izmir Katip Celebi University, Çiğli, Izmir 35620, Turkey
[g] Faculty of Engineering, Metallurgical and Materials Engineering Department, Manisa Celal Bayar University, Muradiye, Manisa 45140, Turkey

ARTICLE INFO

Keywords:
Additive manufacturing
Electron beam melting
Ti-6Al-4V
Surface modification
Bioactivity

ABSTRACT

This work aimed to comprehensively assess the influence of various surface modifications on the formation of apatite ability for EBM Ti-6Al-4V alloy. Sandblasting (S), acid-etching (E), sandblasting and acid-etching (SE), anodization (NA), micro-arc oxidations in 1 M H_2SO_4 solution (SM) and 1 M H_3PO_4 solution (PM) methods were applied to modify electron beam melted (EBM) Ti-6Al-4V surface. The α/α'-Ti structures and TiO_2 phases were detected by XRD. The surface roughness (R_a) values ranged from 0.25 μm and 2.86 μm. The wettability of samples was between around 25° and 104° The SM sample possessed the lowest contact angle. *In vitro* tests were employed in the simulated body fluid (SBF) solution for 28 days. The samples with different surface textures demonstrated bioactive behaviors. *In vitro* test results showed that apatite layers formed on the surfaces. The SM sample exhibited good apatite formation ability when the Ca/P ratios were considered. The apatite formation for the SM sample might derive from high roughness, low contact angle value, the existence of Ti-OH groups, and anatase and rutile phases. The SM can be implemented to boost bioactivity on EBM Ti-6Al-4V alloys.

1. Introduction

Titanium-based alloys have been the most crucial materials which are remarkably utilized in diverse industrial application fields such as aviation [1], marine [2], biomedical [3] due to their low density, high corrosion resistance, outstanding mechanical properties, good toughness and good biocompatibility over the last four decades [4]. Among these Ti alloys and application fields, the Ti-6Al-4V alloy attracts great attention. As mentioned above, it has become the most common alloy as a biomaterial due to its specific properties. Even though Ti-6Al-4V alloy possesses favorable characteristic features to be used as an implant material for the replacement of human body parts, Ti-based alloys have failed after the implantation process [5]. Bare Ti-based alloys lack integration with host tissue. Ti-based materials have been directly restricted as implant materials due to their biological inertness. The existence of biological inertness retards osseointegration between the implant and bone [6–8]. Therefore, many surface modifications have been applied, such as alkaline treatment [9], sandblasting [10], acid-etching [11], anodization [12], plasma electrolytic oxidation (PEO) [13], micro-arc oxidation (MAO) [14] to improve the bioactivity of Ti-based materials. These surface modifications play a profound role in accelerating and facilitating biological responses between the implants and bones. The production of these Ti-based materials is another significant factor that should be considered in terms of their shape and form to be used as an implant. Therefore, different type of manufacturing methods have been implemented to produce Ti-based implant materials such as casting [15], powder technology [16], machining [17], additive manufacturing (AM) [12]. Amongst these manufacturing methods, the AM method has recently been utilized to obtain implant materials with complex geometries, such as porous structures, which facilitates the osseointegration process. Electron beam melting (EBM) is one of the AM methods. EBM is a powder bed process of AM in which an electron beam

* Corresponding author at: Faculty of Engineering, Department of Metallurgical and Materials Engineering, Marmara University, Maltepe, Istanbul 34854, Turkey.
E-mail address: selim.demirci8@gmail.com (S. Demirci).

https://doi.org/10.1016/j.surfin.2022.102372
Received 28 February 2022; Received in revised form 16 September 2022; Accepted 21 September 2022
Available online 1 October 2022

is used as an energy source. The EBM technique is taken place under a vacuum [18]. Firstly, metallic powders are laid and spread on the bed platform. Then, the powders on the bed platform are melted by an electron source to produce one layer. After the production of one layer, the powder bed is displaced downwards in the z-direction by one-layer thickness to enable the spread or lay new fresh powders on the first layer to manufacture new layer [19,20]. EBM method offers high precision, material saving, design and production of complex geometry with flexibility and adaptation to individual needs. The EBM enables to manufacture very complex components at low cost and in short time. EBM provides huge potential for mass production of high quality products. EBM reduces production processes and cost, thereby, it has fewer energy needs overall. The processes of the EBM method, as compared to traditional manufacturing, are more efficient and significantly reduce the environmental impact of waste products [18,21]. As mentioned above, applying EBM Ti-6Al-4V alloys as implant materials has gained much attention because of providing convenience for fabricating desired shapes and forms, such as porous structures. Hence, Ti-6Al-4V alloys have been fabricated by the EBM method for biomedical applications. Lately, Ti-6Al-4V alloys have been manufactured by the EBM method to investigate and study their mechanical, corrosion, tribology, and biological properties. For instance, Ramskogler et al. [22] produced Ti-6Al-4V alloy with EBM technique. Then, they modified the surface of the alloys by using electron beam welding machine (EBW) at different beam current and velocity to create a surface topology for the investigation of cell proliferation. The surface obtained at 0.8 mA and 341 mm/s showed the best cell spreading and proliferation. Yin and co-workers [23] manufactured porous Ti-6Al-4V alloy via the EBM technique. The porous Ti-6Al-4V alloy was treated by ultraviolet photofunctionalization. The results exhibited that the osseointegration of porous Ti-6Al-4V improved after the surfaces' ultraviolet photofunctionalization. Li et al. [24] manufactured porous Ti-6Al-4V alloy. The porous Ti-6Al-4V alloy was exposed to alkali treatment in 10 M NaOH aqueous solution at 60°C for 24 h in order to enhance bioactivity. After that, the *in-vitro* and *in-vivo* experiments were carried out. The findings pointed out that the produced porous EBM Ti-6Al-4V samples boosted apatite formation, cell attachment, viability, cell proliferation as well as *in-vivo* properties. Chudivona et al. [25] fabricated porous Ti-6Al-4V alloy by using the EBM technique. Calcium phosphate nanoparticles (CaPNPs) was applied to alter surface property for porous EBM Ti-6Al-4V alloy to investigate the biological properties. The authors concluded that the change of surface feature enhanced the biocompatibility and increased the osseointegration process. As can be understood from the example studies about surface modification of EBM Ti-6Al-4V for bioactivity application, the comparison of the EBM Ti-6Al-4V alloy in terms of apatite formation ability after surface modification has not been reported. Within this framework, for the first time we applied comprehensive surface modification techniques on Ti-6Al-4V alloy produced via EBM method so as to analyze, compare and evaluate the apatite formation ability. Sandblasting (S), acid etching (E), anodization (NA), sandblasting and acid etching (SE), micro-arc oxidations in 1 M H_2SO_4 (SM) and in 1 M H_3PO_4 (PM) methods were performed on EBM Ti-6Al-4V alloys. These surface modification methods are the most significant for controlling of the surface morphology, roughness, wettability and adhesion of layers in order to functionalize biomaterials. The microstructure, surface roughess, topography and wettability properties of EBM Ti-6Al-4V alloy were analysed and characterized. Moreover, apatite ability experiments were carried out in order to investigate bioactivity performances of surfaces.

2. Materials and methods

2.1. Material and manufacturing

Ti-6Al-4V alloy was obtained via the electron beam manufacturing (EBM) process. The Arcam Q20 machine (EBM theme 5.2.24) was used to manufacture samples. The process parameters are given in Table 1. The samples with dimensions of 145 mm in length and 20 mm in diameter were built vertically by assembling the layers along the z-axis perpendicular to the plate given in Fig. S1. Ti-6Al-4V powder sizes ranged from 45 to 106 μm. The chemical composition of the Ti-6Al-4V powder is shown in Table 1. The preheating temperature for the building plate was around 700°C, and a partial vacuum of 5×10^{-4} mbar was applied during the process. A machining process was applied to alloys after EBM manufacturing.

2.2. Surface modification of alloys

The EBM Ti-6Al-4V was cut into discs 2 cm in diameter and 5 mm in height. Then, SiC papers between 80 and 1200 grits were utilized to grind Ti-6Al-4V alloys. Later, acetone, ethanol, and distilled water were used to clean the surface of Ti-6Al-4V alloys for 15 min. Hydrofluoric acid (HF) and nitric acid (HNO_3) were mixed to obtain a solution to remove natural oxide layers prior to the modifications. The Ti-6Al-4V alloys were modified via sandblasting (S), acid-etching (E), sandblasting and acid-etching (SE), anodization (NA), micro-arc oxidations in 1 M H_2SO_4 (SM), and in 1 M H_3PO_4 (PM) methods. Al_2O_3 particles were sprayed for 2 min in the sandblasting method. A mixture of HCl/H_2SO_4 solutions was utilized in the acid etching process for 10 min. The anodization process was conducted at 20 V in 0.5 wt% HF solution using a power supply at ambient temperature for 30 min. Finally, two separate micro-arc oxidations were conducted at 400 V for 5 min in 1 M H_2SO_4 and 1 M H_3PO_4 solutions. The distance between electrodes was adjusted to be 3 cm for both anodization and micro-arc oxidation processes. The experimental design and surface modification processes are depicted in Fig. 1. Also, the surface modification methods and final photographs of samples after modifications are given in Table 2.

2.3. Material characterization

The microstructure analysis of EBM Ti-6Al-4V alloys was done using an optical microscope (Nikon Eclipse ME600 mode). The phase analysis of EBM Ti-6Al-4V alloys was carried out via X-ray diffraction (Rigaku, Japan, CuKα, $\lambda = 0.1542$ nm). The morphology and elemental analysis were characterized by a scanning electron microscope (SEM, Carl Zeiss 300 VP) equipped with an X-ray spectrometer (EDS). The surface topography and roughness of EBM Ti-6Al-4V alloys were analyzed via a surface profilometer (Ambios XP-2). The wettability of EBM Ti-6Al-4V alloys was measured using an optical tensiometer (Theta Lite). FTIR spectra were obtained through Fourier transform infrared spectroscopy (Perkin Elmer Spectrum II). Tests of apatite formation ability were performed in the simulated body fluid (SBF) solution prepared according to reference [26]. The modified samples were soaked in 100 mL of the solution for 28 days at 37°C. After immersion, the samples were gently rinsed and examined by FTIR and SEM devices.

Table 1
Process parameters and alloy composition for EBM Ti-6Al-4V alloy.

Parameters	Preheat [1/2]	Melting [Outer contour/ Inner contour/Hatch]
Average current [mA]	0/13.95	-
Focus offset [mA]	44	6 / 6 / 45
Speed [mm/s]	40500/40500	450 / 450 / -
Current [mA]	36/45	9 / 9 / 28
Speed function	-	- / - / 32
Line offset [mm]	0.4/0.4	- / - / 0.22
Hatch depth [mm]	0.09/0.09	- / - / 0.09
Alloy Composition (wt %)	Ti (balance); Al (5.5–6.75%); V (3.5–4.5%); O (< 2000 ppm); N (< 500 ppm); C (< 800 ppm); H (< 150 ppm); Fe (< 3000 ppm)	

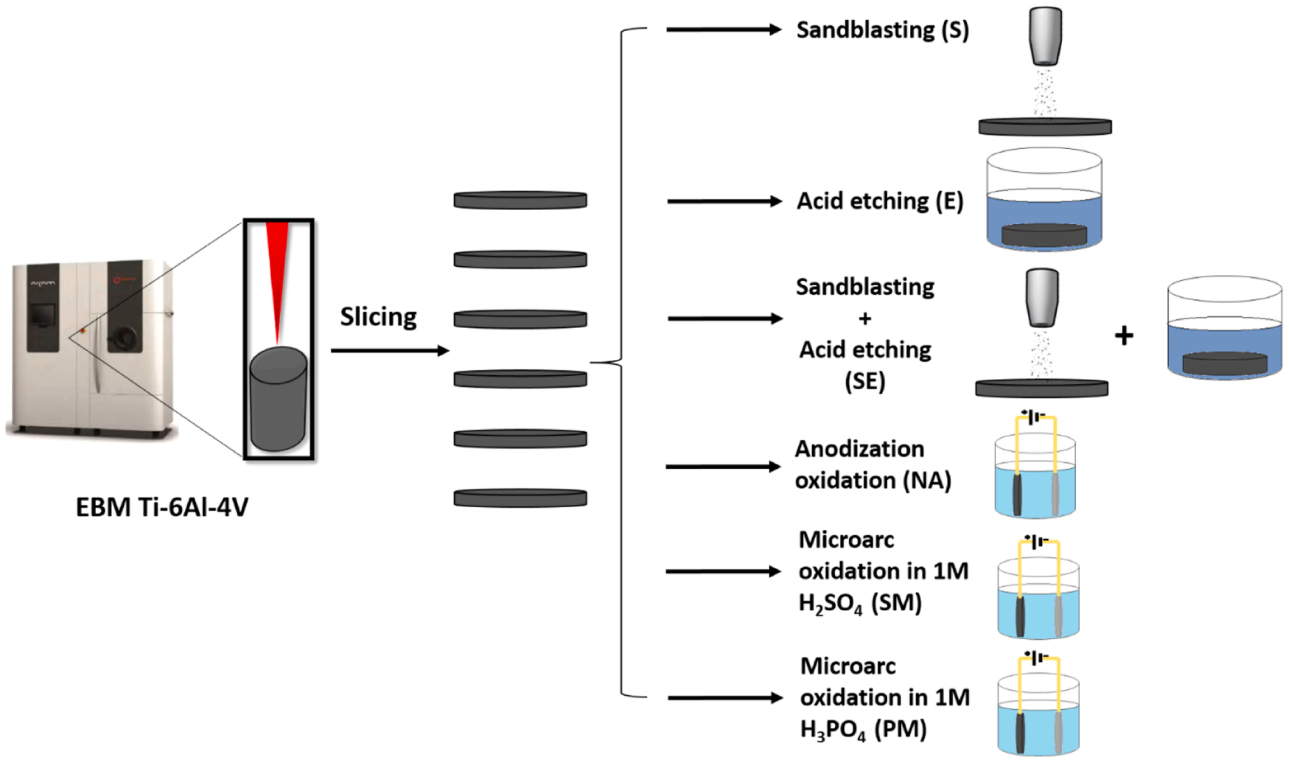

Fig. 1. The experimental design and surface modification processes.

Table 2
Surface modification and photographs of EBM Ti-6Al-4V alloy after modification.

Group	Modification Methods Sandblasting	Acid Etching	Sandblasting+Acid Etching	Anodization	Micro-arc Oxidation in 1 M H_2SO_4	Micro-arc Oxidation in 1 M H_3PO_4
Codes	S	E	SE	NA	SM	PM
Photos						

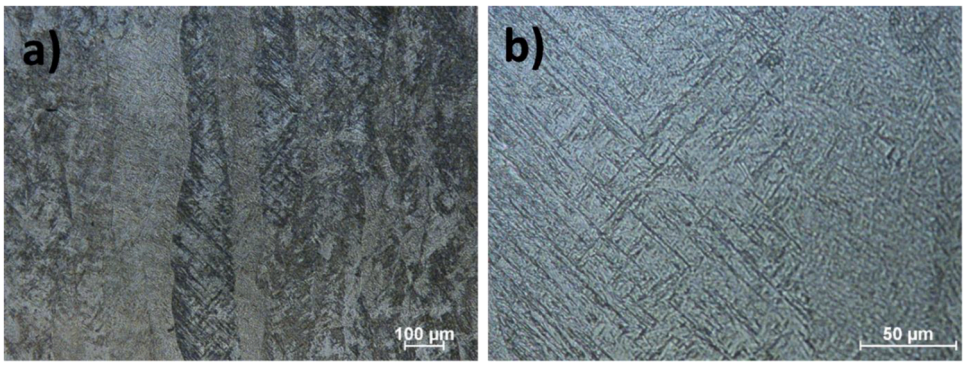

Fig. 2. Optical micrographs of EBM Ti-6Al-4V alloy. (a) Longitudinal cross-section showing columnar beta grains. (b) High magnification longitudinal cross-section image showing needle-like fine α' martensitic laths in the basket-weave structure.

3. Results and discussion

3.1. Microstructure analysis

The optical microscope images of the EBM Ti-6Al-4V, which were taken from the cross-section parallel to the building direction, were shown in Fig. 2. Fig. 2(a) illustrated the columnar growth of prior beta grains along the building direction due to the direction of heat flow. The higher magnification optical image in Fig. 2(b) demonstrated basket-weave morphology, which consisted of a needle-like alpha phase with a small amount of beta phase within the prior beta grains. This microstructure is ~~a~~ typical in the as-built Ti-6Al-4V alloy produced by EBM [12,27].

3.2. X-ray diffraction analysis (XRD)

The results of XRD analysis for EBM Ti-6Al-4V alloys after applying surface modification methods were demonstrated in Fig. 3. As shown in Fig. 3, the α/α'-Ti structures were the dominant phases after modifications. Aside from the existence of α/α' phases, the SM sample possessed anatase and rutile phases, whereas the PM sample had anatase phases. The anatase phase was not observed on the NA sample, even though it was modified by anodization. According to Sul et al. [28], amorphous oxide layers formed after anodization on Ti-based alloys. The formed oxide layers can be detected by XRD analysis as TiO_2 structures after thermal treatment at high temperatures. High temperatures were reached on the sample's surface locally during the micro-arc oxidation process [12]. The high temperature transforms the amorphous phases into crystalline phases. Therefore, TiO_2 phases were observed on PM and SM samples but not on the NA sample. In addition, there was a shift for S and SE samples in the XRD results. The shift towards lower 2θ could appear for S and SE samples in Fig. 3. This shift might be attributed to excessive stress because of sandblasting process [29]. Furthermore, the MAUD (Materials Analysis Using Diffraction) program was used for the Rietveld analysis. According to Rietveld analysis, the weight fraction of α/α'-Ti phases for S, E, SE, and NA samples was 100%. The PM sample contained 62.12% α/α'-Ti phases and 37.88% anatase phases by weight, whereas the SM sample possessed 61.46% α/α'-Ti, 4.075% anatase, and 34.45% rutile phases.

3.3. Surface morphology

Fig. 4 depicted the surface morphologies of EBM Ti-6Al-4V alloy after surface modification processes. As seen in Fig. 4, different surface topographies and morphologies were obtained. The S sample had an irregular coarse and rough surface composed of pits, cavities, and valleys with an irregular edge after sandblasting process in Fig. 4(a). The E sample was similar to the S but less coarse and rough. The morphology of the E sample consisted of micro-pits, valleys, and craters in Fig. 4(b). Fig. 4(c) demonstrated the sandblasted and acid-etched morphology of the EBM Ti-6Al-4V alloy. The SE morphology exhibited crater-like structures and cavities. NA sample had a uniform, homogenous and smooth morphology. The amorphous nanopores can be observed in Fig. 4(d). Fig. 4(e) displayed the surface morphology of EBM Ti-6Al-4V alloy after micro-arc oxidation in the H_2SO_4 solution. As seen in Fig. 4 (e), SM revealed dense circular volcano-like pores. These pores were formed and distributed uniformly and homogeneously on the EBM Ti-6Al-4V alloy. The diameter of pores ranged from 100 nm to 1 μm for the SM sample. The morphology of the PM sample was shown in Fig. 4 (f), obtained in the H_3PO_4 solution. The pore structures with different sizes were observed for the PM sample. The quantity and density of pores on PM samples were lower than that of SM samples. The pore sizes enlarged on the PM sample after the process in which the diameter was between 500 nm and about 5 μm. These results are in good agreement with the literature [30].

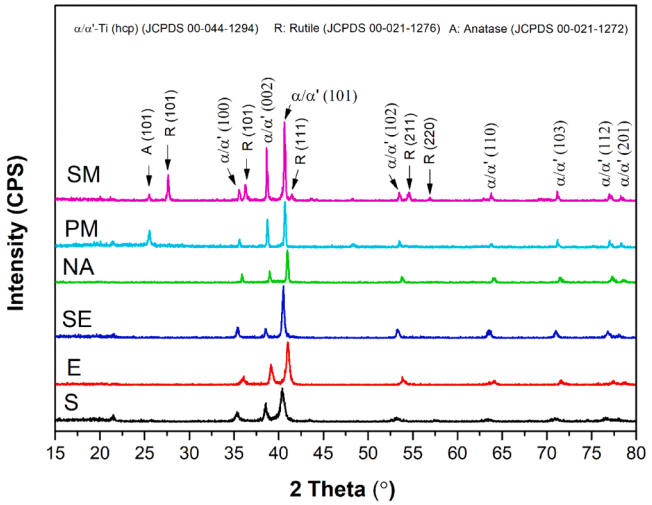

Fig. 3. XRD analysis of EBM Ti-6Al-4V alloys after surface modifications.

3.4. Surface roughness and contact angle measurements

The surface topography, roughness (R_a), and contact angle of EBM Ti-6Al-4V alloys were exhibited in Fig. 5 and Fig. 6, respectively. Based on Fig. 5, the surface-modified samples showed smooth and homogenous roughness patterns on their surfaces. Nevertheless, the applied surface modification methods altered the roughness values. S sample had the highest surface roughness value, approximately 2.86 μm. The roughness value of the E sample was 0.28 μm. On the other hand, the NA sample, whose value was 0.25 μm, showed the lowest surface roughness. The highest roughness for the S sample is expected because of excessive deformation. The sample SE had a lower surface roughness value, about 2.06 μm, than the S samples. The etching process decreased the SE sample's roughness compared to the S sample. As for the SM and PM samples, the surface roughness of the SM sample was nearly 1.38 μm, whereas the PM sample displayed approximately 0.92 μm. Moreover, the contact angles of EBM Ti-6Al-4V alloys were illustrated after surface modifications in Fig. 6. It could be seen that contact angle values were different from one sample to another. The S sample showed hydrophobic behavior with a contact angle of 104.78°. The contact angle of the S sample was the highest. The contact angle value of the NA sample was 104.57°. This value was very close to S one. NA sample displayed hydrophobic behavior because of having high contact angle value. As for E, SE, SM, and PM samples, these samples' surfaces became hydrophilic after modification. The contact angles of E, SE, SM, and PM were 77.06°, 70.93°, 25.84°, and 58.36°, respectively. The SM sample exhibited the lowest contact angle. The surface roughness of samples is given in Table 3. These findings are in good agreement with the literature [12].

The wettability of surfaces is affected by surface chemistry, free energy, surface morphology, and properties of the liquid. Generally, the higher the surface roughness and surface energy, the lower the contact angle value occurs [31,32]. The lowest contact angle value for SM surfaces might stem from surface energy and topological texture. As shown in Fig. 4(e), the SM sample's surface was composed of mainly micron and submicron pore structures, which increased the roughness. In addition, surface chemistry plays a crucial role in wettability properties. The presence of oxide phases on Ti surfaces reduces the contact angle values. Therefore, PM and SM samples had lower contact angles because of Ti-O bonds than others [33,34]. When SM and PM samples were taken into account among themselves, the lower contact angle value for the SM sample than the PM sample was due to the presence of the rutile phase. Because the surface energy of the anatase phase is lower than rutile phases [35], hence SM sample's surface could have high surface energy. The surface properties of SM samples may increase wettability [36–38].

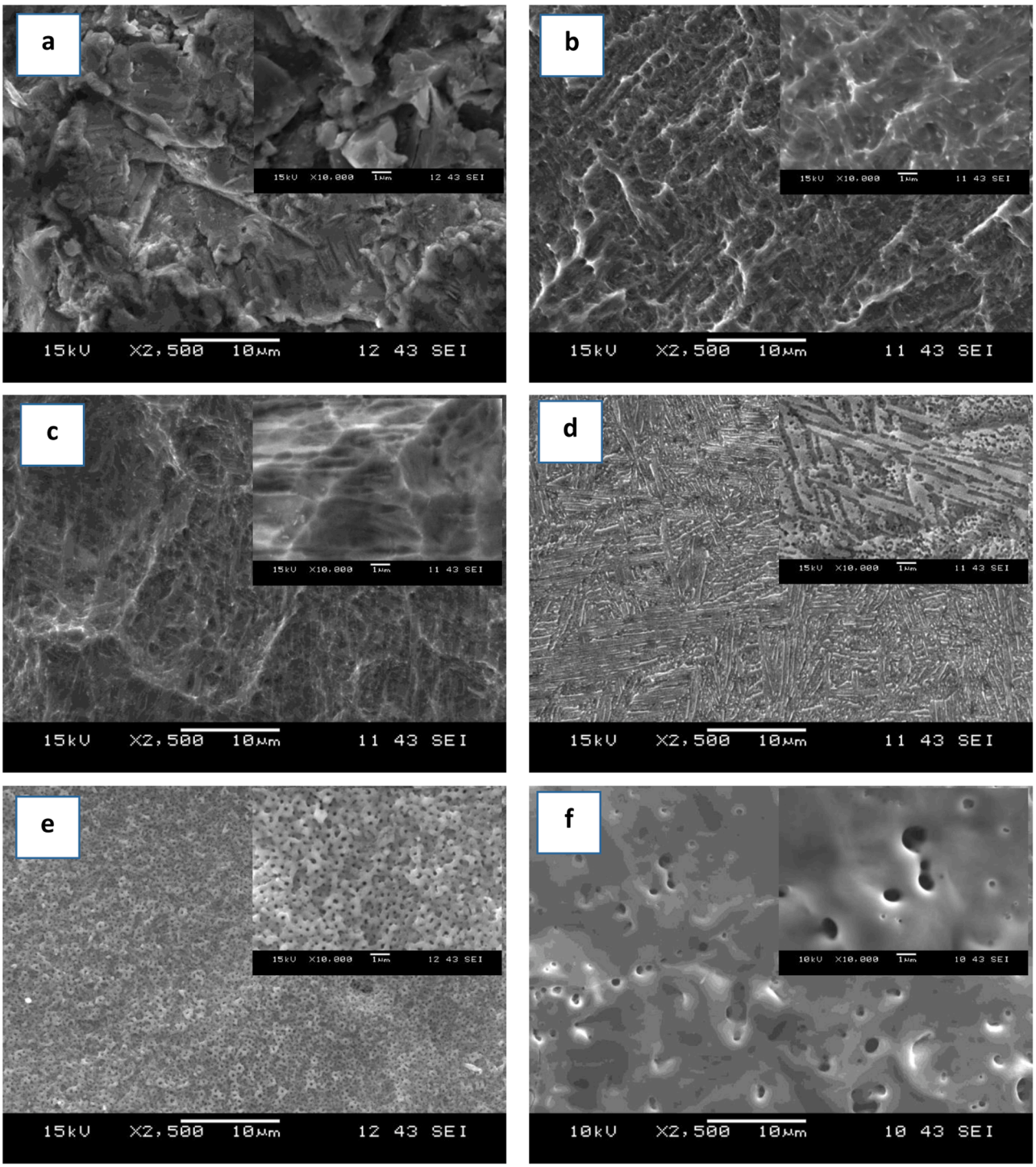

Fig. 4. SEM images of (a) sand-blasted surface (b) etched surface (c) acid-etched surface (d) anodized at 20 V in HF%1 solution (e) micro-arc oxidation at 400 V in 1 M H_2SO_4 solution and (f) micro-arc oxidation at 400 V in 1 M H_3PO_4 solution.

3.5. Apatite forming ability

Apatite forming ability experiments were done to evaluate samples' bioactivity behavior. Fig. 7 showed the SEM micrographs and EDS spectrums of samples' surfaces after immersion in the SBF at 37°C for 28 days. The surfaces of the modified samples demonstrated different bioactive behavior. The apatite forming ability experiments revealed that while the S and PM samples could not form a homogeneous apatite layer, other samples formed a homogeneous, dense and stable apatite layer on their surfaces. As can be seen in Fig. 7(b)-(e), the E, SE, NA, and SM sample surfaces were covered by sponge-like granular structures which were related to apatite formation [39–41]. EDS analysis in Fig. 7 (b)-(e) showed that these granular structures consisted of Ca, P, and O elements. In addition, the stoichiometric value of the Ca/P ratio for E, SE, NA, and SM samples were 1.6, 1.88, 1.56, and 1.72, respectively, as seen in Table 3. The theoretical stoichiometric ratio of Ca and P ions for hydroxyapatite and human bone are 1.67 and 1.5, respectively. Generally, the atomic ratio of Ca and P ions for apatite structures formed in SBF solution ranges between 1.4 and 2.0 [42,43]. The difference in the value of the Ca/P ratio generally originates from occupations of PO_4^{-3}

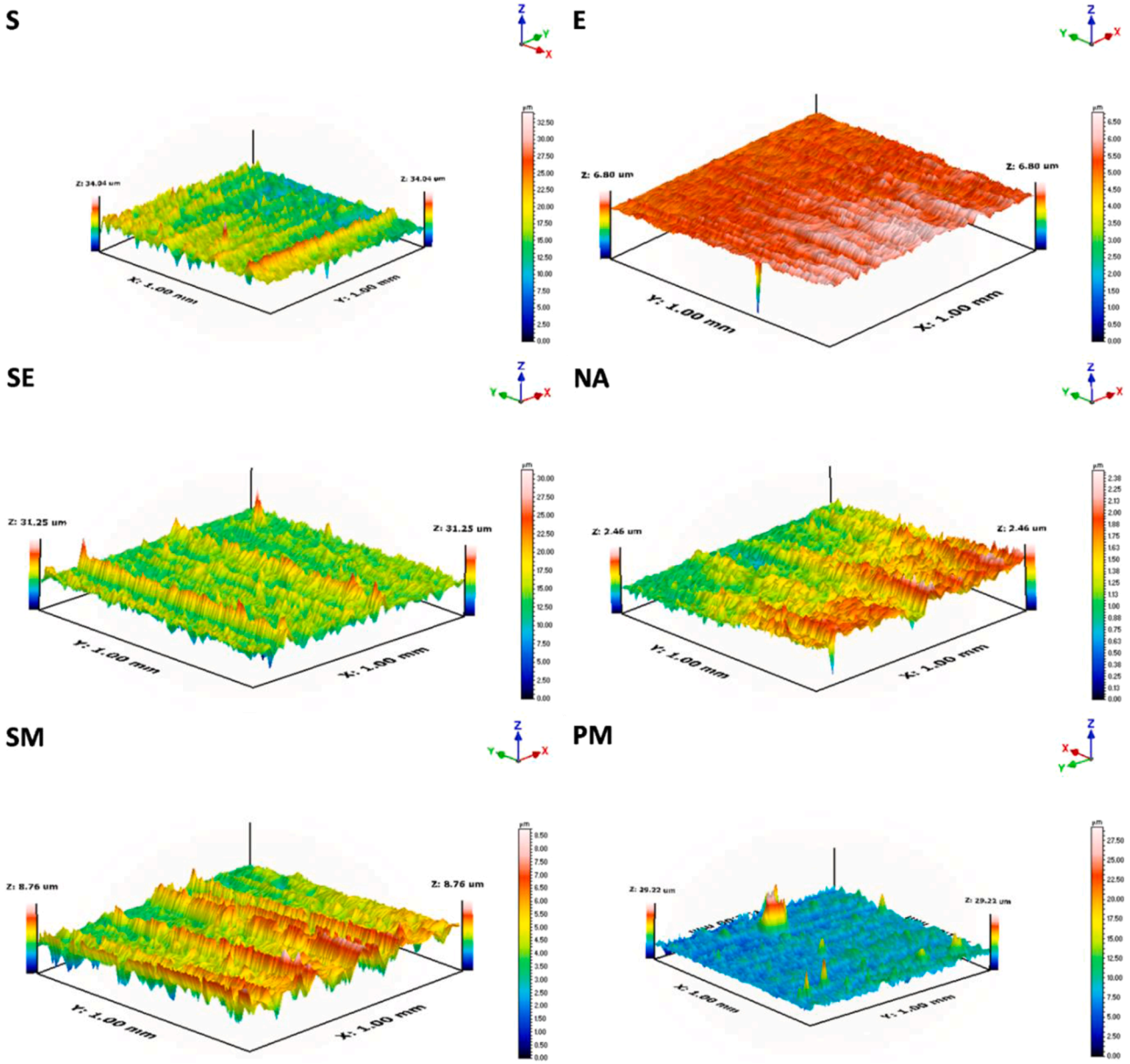

Fig. 5. The surface roughness and topography images of the EBM Ti-6Al-4V alloys after surface modifications.

and CO_3^{-2} ion sites in apatite structure [44]. Hence, it can be expected to obtain different Ca/P ratios for samples in our study owing to various surface modification ways. The apatite layer on the surface of S and PM samples did not form and spread as desired, although EDS analysis revealed that there were Ca and P elements along with Ti, Al, and O, as seen in Fig. 7(a) and (f). The formation of the apatite layer on the surfaces of S and PM samples was weak and low. The Ca/P ratios for S and PM samples were calculated to be 5.09 and 1, respectively, which relates to unstable Ca-P deposition or formations. Hacioglu et al. [42] examined the bioactivity of sandblasted Ti-6Al-4V samples in an SBF environment for 21 days. They concluded that sandblasted samples could not form a uniform and homogenous apatite layer like our result. Also, in the case of the PM sample, Song et al. [30] produced oxide films by anodic spark oxidation in the H_2SO_4 and H_3PO_4 solutions and evaluated the bioactivity of the samples. Results showed that while the oxide films produced in the H_2SO_4 solution formed a stable and homogeneous apatite layer, films produced in the H_3PO_4 solution failed to form an apatite layer. The ability of apatite formation is significantly dependent on the chemical properties of the surface. It could be stated that the apatite formation on Ti alloys mainly originates from the presence of Ti-OH groups, which act as nucleation sites for Ca^{+2} ions [45]. Wu et al. [40] stated that the presence of Ti-OH groups on the surfaces played a vital role in forming the apatite layer owing to acting as nucleation sites. Confirmation of the presence of Ti-OH groups on the surfaces after modification is usually performed by FTIR analysis according to the literature [46,47]. The FTIR spectra of surface-modified samples after 10 days in SBF solution were given in Fig. 8. It could be seen from Fig. 8 that the band centered at about 1100 cm^{-1} might be ascribed to the formation of Ti-OH groups [47]. The higher the band intensity at around 1100 cm^{-1}, the more Ti-OH formation is. As seen in Fig. 8, the SM sample showed the highest intensity at around 1100 cm^{-1}. The results of the FTIR spectra were in good agreement with the apatite ability of samples. Based on the information mentioned above, it was seen that the formation of apatite did not occur due to the lack of Ti-OH groups on the surface of the S sample. Therefore, the apatite layer did not form on the entire surface of the S sample. The same explanation could be valid for the PM sample. Even though both anatase and rutile phases coexist on the surfaces, if the Ti-OH groups did not exist, the apatite formation layers would be too

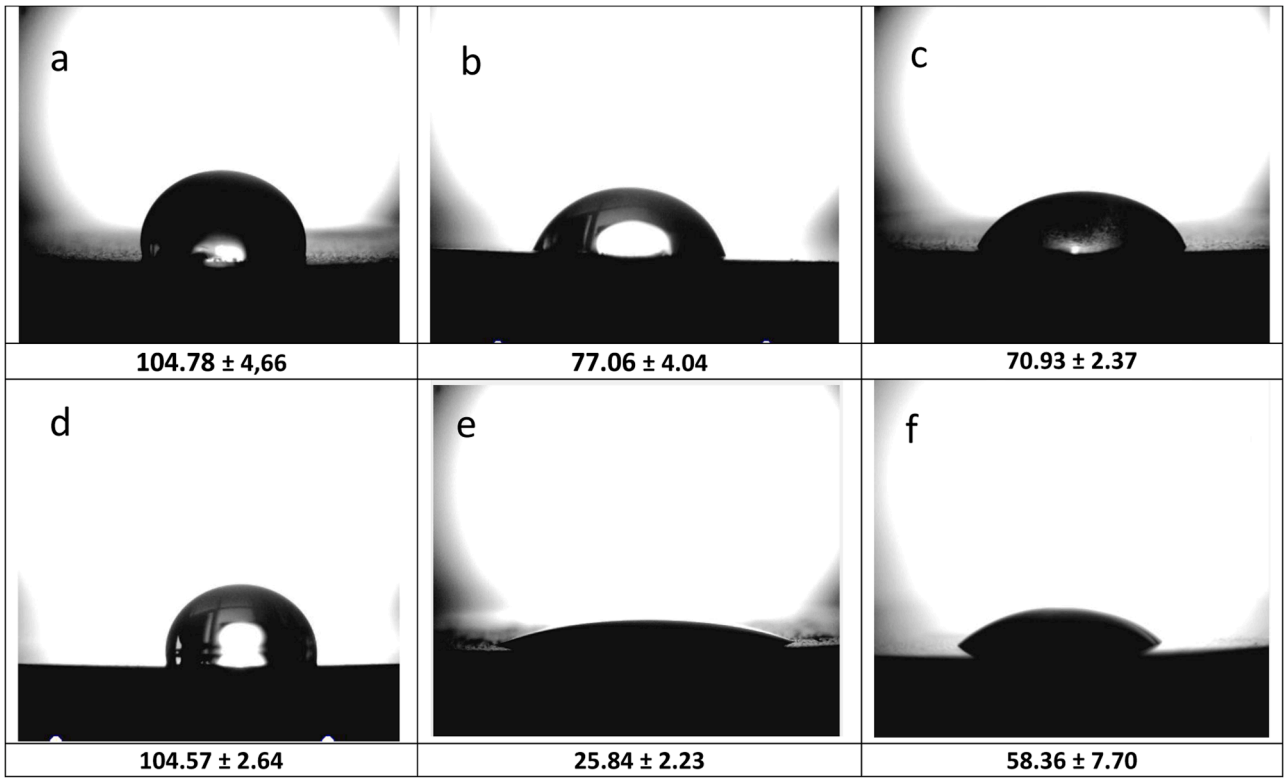

Fig. 6. Contact angle values of (a) sand-blasted surface (b) etched surface (c) sand-blasted + acid-etched surface (d) anodized at 20 V in HF%1 solution (e) micro-arc oxidation at 400 V in 1 M H_2SO_4 solution and (f) micro-arc oxidation at 400 V in 1 M H_3PO_4 solution.

Table 3
Ca/P ratio of surfaces obtained from EDS analysis and surface roughness values of samples.

	S	E	SE	NA	SM	PM
Ca/P Ratio	5,09	1,6	1,88	1,56	1,72	1
R_a	2.86	0.28	2.06	0.25	1.38	0.92

weak and rare on the surfaces. Furthermore, Kang and coworkers [48] noted that although there was anatase phases, the lack of the formed Ti-OH types structures and groups slows down rapid nucleation and growth rates of apatite formation on the surface of Ti-6Al-4V alloy after PEO process. Thus, the lack of apatite formation in the PM sample might be caused by a lack of Ti-OH groups. In addition, the micro-arc oxidation of Ti alloys in H_3PO_4 solution might lead to the formation of superoxide ions, which can prevent apatite nucleation or obtaining compact surface morphology [49,50]. As for E and SE samples, the apatite layers formed and dispersed on the surfaces. Zhang et al. [41] subsequently modified the surface of Ti-6Al-4V samples with sandblasting and acid-etching methods. Results showed that modified surfaces not only increased their wettability but also improved their bioactivity. Similar results were observed in our study for SE and E samples in Fig. 7(b) and (c), and Ca, P, and O elements were detected by EDS analysis. The values of the Ca/P ratio for E and SE samples were estimated to be 1.6 and 1.88, respectively. NA sample also had very uniform and dense apatite layers. Although S and NA samples have similar wettability properties, the formation of an apatite layer on NA sample occurred in Fig. 7(d). The value of Ca/P ratio for NA sample was found to be 1.56. Nhuyen et al. [51] produced different surface properties on the Ti-6Al-4V alloys with anodic treatment in various solutions. They stated that various bioactive surfaces could be obtained by anodic treatment depending on surface chemistry and phase structure. The amorphous TiO or Ti-OH structures might boost the formation of apatite layers after anodization in this study [52]. Lately, the surface feature of the SM sample resembled the NA sample. The Ca/P ratio of the SM sample was 1.72. Within this framework, the results showed that the SM sample had the closest Ca/P ratio value to the hydroxyapatite structure. The SM sample showed the best apatite formation layers. There could be some reasons for better apatite formation. The formation of apatite layers might be strongly influenced by surface chemistry, roughness properties, wettability, and phase [53–55]. Firstly, a rough surface generally assists in the improvement of the bioactivity of materials [56]. When the samples were taken into account, the roughness values followed the *S*>SE>SM>PM>*E*>NA order. SM sample had enough rough surface to promote biological response. Secondly, having a good wettability feature on the surfaces increases the biological activity of biomaterials. As seen in Fig. 6(e), the SM sample showed the lowest contact angle, which easily induced apatite formation [55,57]. Thirdly, the existence of phases on the surface plays a profound role in promoting bioactivity. The presence of anatase and rutile phases stimulates the formation of apatite layers on the surfaces, which soars the bioactivity [40,58,59]. In this study, the SM sample had anatase and rutile phases, whereas the PM sample had only the anatase phase, according to the XRD results. SM sample showed better bioactivity as compared to other samples. Apart from the existence of anatase and rutile phases, as seen in SEM micrographs, the morphologies of the formed apatite layers consisted of granular like structures on the surfaces. The granular type apatite formation is usually stimulated by the presence of TiO or Ti-OH structure and groups on the surfaces of Ti based alloys. Because, granular like apatite formation on the samples' surfaces might be mostly derived from the presence of TiO or Ti-OH which acted as nucleation zones, created by etching, anodization and micro-arc oxidation methods.

FTIR analysis of the samples after immersion in SBF for 28 days is shown in Fig. 9. According to the obtained peaks, all samples showed similar bands, and they were related to phosphate and hydroxyl functional groups, which indicated apatite formation. Bands at around 1045 cm^{-1} and 1061 cm^{-1} were attributed to P-O vibrations of phosphate groups (PO_4^{3-}) [60,61]. The peak at around 875 cm^{-1} could belong to

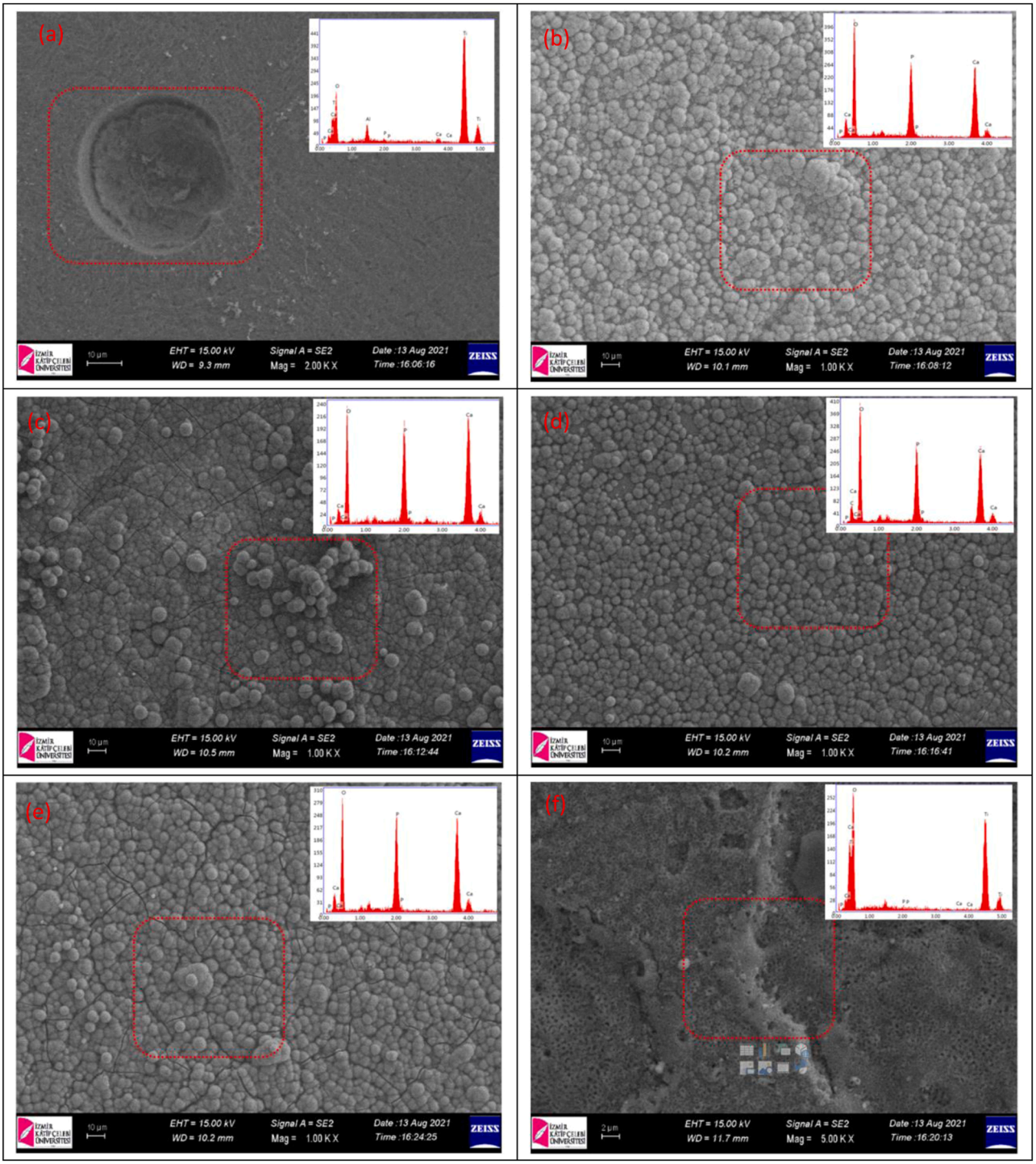

Fig. 7. SEM image and EDS analysis of selected area of (a) S sample, (b) E sample, (c) SE sample, (d) NA sample, (e) SM sample and (f) PM sample.

the carbonate CO_3^{2-} or HPO_4^{2-} groups. The band at 875 cm^{-1} consisted of the joint, which was related to the contribution of CO_3^{2-} and HPO_4^{2-}. Because CO_3^{2-} functional groups partially replaced the PO_4^{3-} ions into apatite lattice, B-type apatite was formed [62,63]. Also, the functional group bands at around 875 cm^{-1} are the characteristic bands of the apatite structure formed after SBF immersion [60,64]. The detected band at around 2910 cm^{-1} may be due to HPO_4^{2-} [65]. The peak at around 1405 cm^{-1} consisted of asymmetric stretching of the C—O bond. Also, the bands at 2981 cm^{-1} and 3680 cm^{-1} corresponded to the stretching mode of the hydroxyl group, which indicated water absorption and apatite formation [61,66]. In conclusion, all samples showed functional groups that indicated Ca/P precipitation or apatite layer formation, but SEM analysis revealed that some samples had relatively more bioactive sites.

4. Conclusion

In conclusion, the EBM method was used to produce Ti-6Al-4V alloy. The surfaces of Ti-6Al-4V alloys were modified via sandblasting (S), acid-etching (E), sandblasting and acid-etching (SE), anodization (NA), micro-arc oxidations in 1 M H_2SO_4 (SM), and in 1 M H_3PO_4 (PM) methods. The α/α'-Ti, anatase, and rutile phases were detected. The

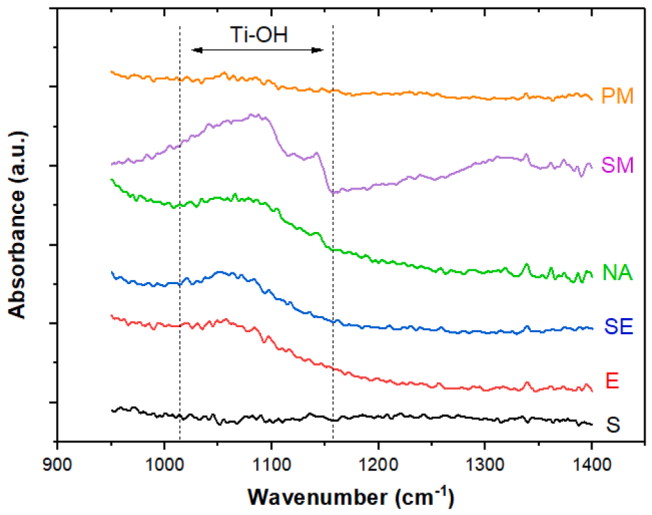

Fig. 8. FTIR spectra of the surfaced modified samples soaked in SBF solution for 10 days.

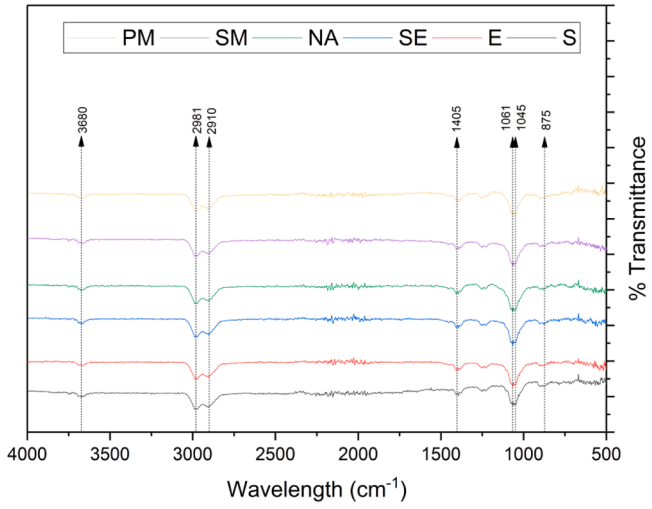

Fig. 9. FTIR analysis of samples after 28 days immersion in the SBF.

surface roughness of samples followed the *S*>SE>SM>PM>*E*>NA order. The surface roughness values changed between 2.86 μm and 0.25 μm. The contact angle values of E, SE, SM, and PM were 77.06°, 70.93°, 25.84°, and 58.36°, whereas S and NA samples had 104.78° and 104.57°, respectively. Apatite formation ability experiments were done in SBF solution for 28 days. The apatite formation results showed that the ability of apatite formation significantly dependent on the surface properties. However, the surface properties were not always enough to form efficient apatite structures on the surfaces. Even though the SM sample did not show the best wettability and highest roughness, the SM sample exhibited better apatite formation ability because of the better formation of Ti-OH groups on the surface. FTIR analysis validated that different amounts of Ti-OH were formed on the sample surfaces. The SM sample exhibited the highest band intensity at around 1100 cm^{-1}. The value of the Ca/P ratio for the SM sample was 1.72, which was very close to the theoretical value of hydroxyapatite. The surface properties profoundly affect the formation of Ti-OH groups on the surface. The micro-arc oxidation process for EBM Ti-6Al-4V alloys in H_2SO_4 solution could be a better modification choice for apatite formation.

CRediT authorship contribution statement

Selim Demirci: Conceptualization, Methodology, Data curation, Formal analysis, Funding acquisition, Methodology, Writing – original draft, Writing – review & editing. **Tuncay Dikici:** Resources, Investigation, Supervision, Validation, Visualization. **Mehmet Masum Tünçay:** Formal analysis, Visualization, Writing – review & editing. **Ramazan Dalmış:** Formal analysis, Writing – original draft, Writing – review & editing. **Nusret Kaya:** Software, Supervision, Validation, Visualization, Writing – review & editing. **Kürşat Kanbur:** Formal analysis, Visualization, Writing – review & editing. **Fatih Sargın:** Formal analysis, Visualization, Writing – review & editing. **Arif Nihat Güllüoğlu:** Supervision, Validation, Visualization, Writing – review & editing.

Declaration of Competing Interest

The authors declare that they have no known competing financial interests or personal relationships that could have appeared to influence the work reported in this paper.

Acknowledgments

This work is supported by Marmara University (Bapko project no: FDK-2022-10185).

Supplementary materials

Supplementary material associated with this article can be found, in the online version, at doi:10.1016/j.surfin.2022.102372.

References

[1] D.Y. Pimenov, M. Mia, M.K. Gupta, A.R. Machado, Í.V. Tomaz, M. Sarikaya, S. Wojciechowski, T. Mikolajczyk, W. Kapłonek, Improvement of machinability of Ti and its alloys using cooling-lubrication techniques: a review and future prospect, J. Mater. Res. Technol. 11 (2021) 719–753, https://doi.org/10.1016/j.jmrt.2021.01.031.

[2] I. Gurrappa, Characterization of titanium alloy Ti-6Al-4V for chemical, marine and industrial applications, Mater. Charact. 51 (2003) 131–139, https://doi.org/10.1016/j.matchar.2003.10.006.

[3] L.-.C. Zhang, L.-.Y. Chen, A review on biomedical titanium alloys: recent progress and prospect, Adv. Eng. Mater. 21 (2019), 1801215, https://doi.org/10.1002/adem.201801215.

[4] Y. Chang, W. Lu, J. Guénolé, L.T. Stephenson, A. Szczpaniak, P. Kontis, A. K. Ackerman, F.F. Dear, I. Mouton, X. Zhong, S. Zhang, D. Dye, C.H. Liebscher, D. Ponge, S. Korte-Kerzel, D. Raabe, B. Gault, Ti and its alloys as examples of cryogenic focused ion beam milling of environmentally-sensitive materials, Nat. Commun. 10 (2019) 942, https://doi.org/10.1038/s41467-019-08752-7.

[5] M. Geetha, A.K. Singh, R. Asokamani, A.K. Gogia, Ti based biomaterials, the ultimate choice for orthopaedic implants—a review, Prog. Mater Sci. 54 (2009) 397–425, https://doi.org/10.1016/j.pmatsci.2008.06.004.

[6] B. Ren, Y. Wan, C. Liu, H. Wang, M. Yu, X. Zhang, Y. Huang, Improved osseointegration of 3D printed Ti-6Al-4V implant with a hierarchical micro/nano surface topography: an *in vitro* and *in vivo* study, Mater. Sci. Eng. C 118 (2021), 111505, https://doi.org/10.1016/j.msec.2020.111505.

[7] S. Rastegari, E. Salahinejad, Surface modification of Ti-6Al-4V alloy for osseointegration by alkaline treatment and chitosan-matrix glass-reinforced nanocomposite coating, Carbohydr. Polym. 205 (2019) 302–311, https://doi.org/10.1016/j.carbpol.2018.10.082.

[8] W. Liu, S. Liu, L. Wang, Surface modification of biomedical titanium alloy: micromorphology, microstructure evolution and biomedical applications, Coatings 9 (2019) 249, https://doi.org/10.3390/coatings9040249.

[9] J. Xiong, Y. Li, X. Wang, P. Hodgson, C.e. Wen, Mechanical properties and bioactive surface modification via alkali-heat treatment of a porous Ti–18Nb–4Sn alloy for biomedical applications, Acta Biomater. 4 (2008) 1963–1968, https://doi.org/10.1016/j.actbio.2008.04.022.

[10] S. Demirci, T. Dikici, A.N. Güllüoğlu, Micro/nanoscale surface modification of Ti-6Al-4V alloy for implant applications, J. Mater. Eng. Perform. (2021), https://doi.org/10.1007/s11665-021-06232-y.

[11] D. Wang, G. He, Y. Tian, N. Ren, W. Liu, X. Zhang, Dual effects of acid etching on cell responses and mechanical properties of porous titanium with controllable open-porous structure, J. Biomed. Mater. Res. B Appl. Biomater. 108 (2020) 2386–2395, https://doi.org/10.1002/jbm.b.34571.

[12] S. Demirci, R. Dalmış, T. Dikici, M.M. Tünçay, N. Kaya, A.N. Güllüoğlu, Effect of surface modifications of additively manufactured Ti-6Al-4V alloys on apatite

formation ability for biomedical applications, J. Alloy. Compd. 887 (2021), 161445, https://doi.org/10.1016/j.jallcom.2021.161445.
[13] B.L. Pereira, G. Beilner, C.M. Lepienski, E.S. Szameitat, B.S. Chee, N.K. Kuromoto, L.L. dos Santos, I. Mazzaro, A.P.R.A. Claro, M.J.D. Nugent, Oxide coating containing apatite formed on Ti-25Nb-25Ta alloy treated by Two-Step Plasma Electrolytic Oxidation, Surf. Coat. Technol. 382 (2020), 125224, https://doi.org/10.1016/j.surfcoat.2019.125224.
[14] H.J. Chu, C.-.J. Liang, C.-.H. Chen, J.-.L. He, Optical emission spectroscopic determination of the optimum regions for micro-arc oxidation of titanium, Surf. Coat. Technol. 325 (2017) 166–173, https://doi.org/10.1016/j.surfcoat.2017.06.022.
[15] M. Kaseem, H.-.C. Choe, Electrochemical and bioactive characteristics of the porous surface formed on Ti-xNb alloys via plasma electrolytic oxidation, Surf. Coat. Technol. 378 (2019), 125027, https://doi.org/10.1016/j.surfcoat.2019.125027.
[16] Y. Zhang, K. Chu, S. He, B. Wang, W. Zhu, F. Ren, Fabrication of high strength, antibacterial and biocompatible Ti-5Mo-5Ag alloy for medical and surgical implant applications, Mater. Sci. Eng. C 106 (2020), 110165, https://doi.org/10.1016/j.msec.2019.110165.
[17] Y. Kaynak, A. Gharibi, U. Yılmaz, U. Köklü, K. Aslantaş, A comparison of flood cooling, minimum quantity lubrication and high pressure coolant on machining and surface integrity of titanium Ti-5553 alloy, J. Manuf. Process. 34 (2018) 503–512, https://doi.org/10.1016/j.jmapro.2018.06.003.
[18] J.A. Tamayo, M. Riascos, C.A. Vargas, L.M. Baena, Additive manufacturing of Ti-6Al-4V alloy via electron beam melting for the development of implants for the biomedical industry, Heliyon 7 (2021) e06892, https://doi.org/10.1016/j.heliyon.2021.e06892.
[19] S.-.X. Liang, X. Wang, W. Zhang, Y.-.J. Liu, W. Wang, L.-.C. Zhang, Selective laser melting manufactured porous Fe-based metallic glass matrix composite with remarkable catalytic activity and reusability, Appl. Mater. Today 19 (2020), 100543, https://doi.org/10.1016/j.apmt.2019.100543.
[20] L.-.Y. Chen, S.-.X. Liang, Y. Liu, L.-.C. Zhang, Additive manufacturing of metallic lattice structures: unconstrained design, accurate fabrication, fascinated performances, and challenges, Mater. Sci. Eng. R Rep. 146 (2021), 100648, https://doi.org/10.1016/j.mser.2021.100648.
[21] A.K. Singh, P. Ratrey, A. Astarita, S. Franchitti, A. Mishra, A. Arora, Enhanced cytocompatibility and mechanical properties of electron beam melted Ti-6Al-4V by friction stir processing, J. Manuf. Process. 72 (2021) 400–410, https://doi.org/10.1016/j.jmapro.2021.10.031.
[22] C. Ramskogler, F. Warchomicka, S. Mostofi, A. Weinberg, C. Sommitsch, Innovative surface modification of Ti-6Al-4V alloy by electron beam technique for biomedical application, Mater. Sci. Eng. C 78 (2017) 105–113, https://doi.org/10.1016/j.msec.2017.03.311.
[23] C. Yin, T. Zhang, Q. Wei, H. Cai, Y. Cheng, Y. Tian, H. Leng, C. Wang, S. Feng, Z. Liu, Surface treatment of 3D printed porous Ti-6Al-4V implants by ultraviolet photofunctionalization for improved osseointegration, Bioact. Mater. 7 (2022) 26–38, https://doi.org/10.1016/j.bioactmat.2021.05.043.
[24] X. Li, Y.-.F. Feng, C.-.T. Wang, G.-.C. Li, W. Lei, Z.-.Y. Zhang, L. Wang, Evaluation of biological properties of electron beam melted Ti-6Al-4V implant with biomimetic coating *in vitro* and *in vivo*, PLoS One 7 (2012) e52049, https://doi.org/10.1371/journal.pone.0052049.
[25] E.A. Chudinova, M.A. Surmeneva, A.S. Timin, T.E. Karpov, A. Wittmar, M. Ulbricht, A. Ivanova, K. Loza, O. Prymak, A. Koptyug, M. Epple, R.A. Surmenev, Adhesion, proliferation, and osteogenic differentiation of human mesenchymal stem cells on additively manufactured Ti-6Al-4V alloy scaffolds modified with calcium phosphate nanoparticles, Colloids Surf. B 176 (2019) 130–139, https://doi.org/10.1016/j.colsurfb.2018.12.047.
[26] T. Kokubo, H. Takadama, How useful is SBF in predicting *in vivo* bone bioactivity? Biomaterials 27 (2006) 2907–2915, https://doi.org/10.1016/j.biomaterials.2006.01.017.
[27] C. de Formanoir, S. Michotte, O. Rigo, L. Germain, S. Godet, Electron beam melted Ti-6Al-4V: microstructure, texture and mechanical behavior of the as-built and heat-treated material, Mater. Sci. Eng. A Struct. Mater. 652 (2016) 105–119, https://doi.org/10.1016/j.msea.2015.11.052.
[28] Y.-.T. Sul, C.B. Johansson, Y. Jeong, T. Albrektsson, The electrochemical oxide growth behaviour on titanium in acid and alkaline electrolytes, Med. Eng. Phys. 23 (2001) 329–346, https://doi.org/10.1016/S1350-4533(01)00050-9.
[29] X.P. Ren, H.Q. Li, H. Guo, F.L. Shen, C.X. Qin, E.T. Zhao, X.Y. Fang, A comparative study on mechanical properties of Ti-6Al-4V alloy processed by additive manufacturing vs. traditional processing, Mater. Sci. Eng. A Struct. Mater. 817 (2021), 141384, https://doi.org/10.1016/j.msea.2021.141384.
[30] H.-.J. Song, S.-.H. Park, S.-.H. Jeong, Y.-.J. Park, Surface characteristics and bioactivity of oxide films formed by anodic spark oxidation on titanium in different electrolytes, J. Mater. Process. Technol. 209 (2009) 864–870, https://doi.org/10.1016/j.jmatprotec.2008.02.055.
[31] C.G. Jothi Prakash, R. Prasanth, Approaches to design a surface with tunable wettability: a review on surface properties, J. Mater. Sci. 56 (2021) 108–135, https://doi.org/10.1007/s10853-020-05116-1.
[32] Z. Wang, M. Elimelech, S. Lin, Environmental applications of interfacial materials with special wettability, Environ. Sci. Technol. 50 (2016) 2132–2150, https://doi.org/10.1021/acs.est.5b04351.
[33] B. Feng, J. Weng, B.C. Yang, J.Y. Chen, J.Z. Zhao, L. He, S.K. Qi, X.D. Zhang, Surface characterization of titanium and adsorption of bovine serum albumin, Mater. Charact. 49 (2002) 129–137, https://doi.org/10.1016/S1044-5803(02)00341-8.
[34] J.L. González-Carrasco, S.C. Cifuentes Cuellar, M. Lieblich Rodríguez, 5 - Metals (Eds.), in: K.M. Pawelec, J.A. Planell (Eds.), Bone Repair Biomaterials (Second Edition), Woodhead Publishing, 2019, pp. 103–140.
[35] A.A. Mosquera, J.M. Albella, V. Navarro, D. Bhattacharyya, J.L. Endrino, Effect of silver on the phase transition and wettability of titanium oxide films, Sci. Rep. 6 (2016) 32171, https://doi.org/10.1038/srep32171.
[36] M. Pan, Z. Weng, J. Liu, Effect of positive bias on properties of chitosan coating prepared on micro-arc oxidation surface of Ti-6Al-4V alloy by electrophoretic deposition, Mater. Chem. Phys. 275 (2022), 125257, https://doi.org/10.1016/j.matchemphys.2021.125257.
[37] O. Keles, A. Qadeer, B.S. Yilbas, Wetting state of 3D printed Ti-6Al-4V alloy surface. Advances in Materials and Processing Technologies, 2021, pp. 1–11, https://doi.org/10.1080/2374068X.2021.1912539.
[38] R. Gabor, M. Doubkova, S. Gorosova, K. Malanik, M. Vandrovcova, L. Cvrcek, K. Drobikova, K. Mamulova Kutlakova, L. Bacakova, Preparation of highly wettable coatings on Ti-6Al-4V ELI alloy for traumatological implants using micro-arc oxidation in an alkaline electrolyte, Sci. Rep. 10 (2020) 19780, https://doi.org/10.1038/s41598-020-76448-w.
[39] F. Sargin, G. Erdogan, K. Kanbur, A. Turk, Investigation of *in vitro* behavior of plasma sprayed Ti, TiO2 and HA coatings on PEEK, Surf. Coat. Technol. 411 (2021), 126965, https://doi.org/10.1016/j.surfcoat.2021.126965.
[40] J.-.M. Wu, S. Hayakawa, K. Tsuru, A. Osaka, Low-temperature preparation of anatase and rutile layers on titanium substrates and their ability to induce *in vitro* apatite deposition, J. Am. Ceram. Soc. 87 (2004) 1635–1642, https://doi.org/10.1111/j.1551-2916.2004.01635.x.
[41] Y. Zhang, M. Wu, T. Wang, S. Guo, Fabrication of porous micro-nanostructured networks on Ti-6Al-4V for faster hydroxyapatite deposition in SBF, Mater. Lett. 256 (2019), 126571, https://doi.org/10.1016/j.matlet.2019.126571.
[42] T. Hacioglu, Z. Evis, A. Tezcaner, M.K. Aydınol, Effects of surface pretreatments and coating period on hydroxyapatite coating of Ti-6Al-4V alloy, J. Aust. Ceram. Soc. 56 (2020) 545–557, https://doi.org/10.1007/s41779-019-00364-0.
[43] D.-.M. Liu, T. Troczynski, W.J. Tseng, Water-based sol–gel synthesis of hydroxyapatite: process development, Biomaterials 22 (2001) 1721–1730, https://doi.org/10.1016/S0142-9612(00)00332-X.
[44] H.M. Kim, K. Kishimoto, F. Miyaji, T. Kokubo, T. Yao, Y. Suetsugu, J. Tanaka, T. Nakamura, Composition and structure of apatite formed on organic polymer in simulated body fluid with a high content of carbonate ion, J. Mater. Sci. Mater. Med. 11 (2000) 421–426, https://doi.org/10.1023/A:1008935924847.
[45] H. Takadama, H.-.M. Kim, T. Kokubo, T. Nakamura, XPS study of the process of apatite formation on bioactive Ti-6Al-4V alloy in simulated body fluid, Sci. Technol. Adv. Mater. 2 (2001) 389–396, https://doi.org/10.1016/S1468-6996(01)00007-9.
[46] P. Zhang, Z. Zhang, W. Li, M. Zhu, Effect of Ti-OH groups on microstructure and bioactivity of TiO2 coating prepared by micro-arc oxidation, Appl. Surf. Sci. 268 (2013) 381–386, https://doi.org/10.1016/j.apsusc.2012.12.105.
[47] Y. Chen, X. Zheng, H. Ji, C. Ding, Effect of Ti–OH formation on bioactivity of vacuum plasma sprayed titanium coating after chemical treatment, Surf. Coat. Technol. 202 (2007) 494–498, https://doi.org/10.1016/j.surfcoat.2007.06.015.
[48] J.-.I. Kang, M.-.K. Son, H.-.C. Choe, W.A. Brantley, Bone-like apatite formation on manganese-hydroxyapatite coating formed on Ti-6Al-4V alloy by plasma electrolytic oxidation, Thin Solid Films 620 (2016) 126–131, https://doi.org/10.1016/j.tsf.2016.07.088.
[49] X.-.X. Wang, S. Hayakawa, K. Tsuru, A. Osaka, Improvement of bioactivity of H2O2/TaCl5-treated titanium after subsequent heat treatments, J. Biomed. Mater. Res., 52 (2000) 171–176. 10.1002/1097-4636(200010)52:1<171::AID−JBM22>3.0.CO;2-O.
[50] H. Tsuchiya, J.M. Macak, L. Müller, J. Kunze, F. Müller, P. Greil, S. Virtanen, P. Schmuki, Hydroxyapatite growth on anodic TiO2 nanotubes, J. Biomed. Mater. Res. A 77A (2006) 534–541, https://doi.org/10.1002/jbm.a.30677.
[51] V.-.T. Nguyen, T.-.C. Cheng, T.-.H. Fang, M.-.H. Li, The fabrication and characteristics of hydroxyapatite film grown on titanium alloy Ti-6Al-4V by anodic treatment, J. Mater. Res. Technol. 9 (2020) 4817–4825, https://doi.org/10.1016/j.jmrt.2020.03.002.
[52] A. Wennerberg, T. Albrektsson, On implant surfaces: a review of current knowledge and opinions, Int. J. Oral Maxillofac. Implants 25 (2010) 63–74.
[53] H.M. Kim, T. Himeno, M. Kawashita, T. Kokubo, T. Nakamura, The mechanism of biomineralization of bone-like apatite on synthetic hydroxyapatite: an *in vitro* assessment, J. R. Soc. Interface 1 (2004) 17–22, https://doi.org/10.1098/rsif.2004.0003.
[54] X. Chen, R.-f. Zhu, H. Gao, W.-l. Xu, G.-y. Xiao, C.-z. Chen, Y.-p. Lu, A high bioactive alkali-treated titanium surface induced by induction heat treatment, Surf. Coat. Technol. 385 (2020), 125362, https://doi.org/10.1016/j.surfcoat.2020.125362.
[55] J.I. Rosales-Leal, M.A. Rodríguez-Valverde, G. Mazzaglia, P.J. Ramón-Torregrosa, L. Díaz-Rodríguez, O. García-Martínez, M. Vallecillo-Capilla, C. Ruiz, M. A. Cabrerizo-Vílchez, Effect of roughness, wettability and morphology of engineered titanium surfaces on osteoblast-like cell adhesion, Colloids Surf. A 365 (2010) 222–229, https://doi.org/10.1016/j.colsurfa.2009.12.017.
[56] L.J. Heitz-Mayfield, A. Mombelli, The therapy of peri-implantitis: a systematic review, Int. J. Oral Maxillofac. Implants 29 (Suppl) (2014) 325–345, https://doi.org/10.11607/jomi.2014suppl.g5.3.
[57] L. Fialho, S. Carvalho, Surface engineering of nanostructured Ta surface with incorporation of osteoconductive elements by anodization, Appl. Surf. Sci. 495 (2019), 143573, https://doi.org/10.1016/j.apsusc.2019.143573.
[58] M.D. Roach, R.S. Williamson, I.P. Blakely, L.M. Didier, Tuning anatase and rutile phase ratios and nanoscale surface features by anodization processing onto

titanium substrate surfaces, Mater. Sci. Eng. C 58 (2016) 213–223, https://doi.org/10.1016/j.msec.2015.08.028.
[59] F. Hilario, V. Roche, R.P. Nogueira, A.M.J. Junior, Influence of morphology and crystalline structure of TiO2 nanotubes on their electrochemical properties and apatite-forming ability, Electrochim. Acta 245 (2017) 337–349, https://doi.org/10.1016/j.electacta.2017.05.160.
[60] X. Chen, Y. Li, P.D. Hodgson, C.e. Wen, Microstructures and bond strengths of the calcium phosphate coatings formed on titanium from different simulated body fluids, Mater. Sci. Eng. C 29 (2009) 165–171, https://doi.org/10.1016/j.msec.2008.06.004.
[61] H. Ghomi, M.H. Fathi, H. Edris, Preparation of nanostructure hydroxyapatite scaffold for tissue engineering applications, J. Solgel Sci. Technol. 58 (2011) 642–650, https://doi.org/10.1007/s10971-011-2439-2.
[62] J. Xu, L. Liu, P. Munroe, Z.-.H. Xie, Promoting bone-like apatite formation on titanium alloys through nanocrystalline tantalum nitride coatings, J. Mater. Chem. B 3 (2015) 4082–4094, https://doi.org/10.1039/C5TB00236B.
[63] J. Weng, Q. Liu, J.G.C. Wolke, X. Zhang, K. de Groot, Formation and characteristics of the apatite layer on plasma-sprayed hydroxyapatite coatings in simulated body fluid, Biomaterials 18 (1997) 1027–1035, https://doi.org/10.1016/S0142-9612(97)00022-7.
[64] Q. Wang, C. Han, T. Choma, Q. Wei, C. Yan, B. Song, Y. Shi, Effect of Nb content on microstructure, property and *in vitro* apatite-forming capability of Ti-Nb alloys fabricated via selective laser melting, Mater. Des. 126 (2017) 268–277, https://doi.org/10.1016/j.matdes.2017.04.026.
[65] F. Haftlang, A. Zarei-Hanzaki, H.R. Abedi, The effect of nano-size second precipitates on the structure, apatite-inducing ability and *in-vitro* biocompatibility of Ti-29Nb-14Ta-4.5Zr alloy, Mater. Sci. Eng. C 109 (2020), 110561, https://doi.org/10.1016/j.msec.2019.110561.
[66] E. Ajami, K.-.F. Aguey-Zinsou, Calcium phosphate growth at electropolished titanium surfaces, J. Funct. Biomater. 3 (2012) 327–348. https://www.mdpi.com/2079-4983/3/2/327.